

A Programmable Peptidic Hydrogel Adjuvant for Personalized Immunotherapy in Resected Stage Tumors

Bihan Wu, Juan Liang, Xuejiao Yang, Yu Fang, Nan Kong, Dinghao Chen, and Huaimin Wang*



Cite This: *J. Am. Chem. Soc.* 2024, 146, 8585–8597



Read Online

ACCESS |



Metrics & More

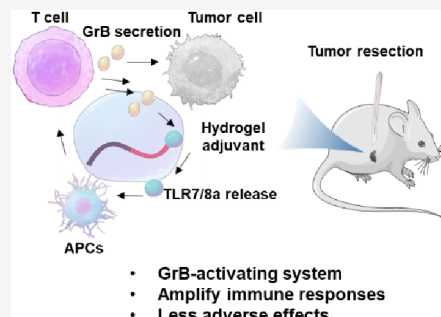


Article Recommendations



Supporting Information

ABSTRACT: Adjuvant treatment after surgical resection usually plays an important role in delaying disease recurrence. Immunotherapy displays encouraging results in increasing patients' chances of staying cancer-free after surgery, as reported by recent clinical trials. However, the clinical outcomes of current immunotherapy need to be improved due to the limited responses, patient heterogeneity, nontargeted distribution, and immune-related adverse effects. This work describes a programmable hydrogel adjuvant for personalized immunotherapy after surgical resection. By filling the hydrogel in the cavity, this system aims to address the limited secretion of granzyme B (GrB) during immunotherapy and improve the low immunotherapy responses typically observed, while minimizing immune-related side effects. The TLR7/8 agonist imidazoquinoline (IMDQ) is linked to the self-assembling peptide backbone through a GrB-responsive linkage. Its release could enhance the activation and function of immune cells, which will lead to increased secretion of GrB and enhance the effectiveness of immunotherapy together. The hydrogel adjuvant recruits immune cells, initiates dendritic cell maturation, and induces M1 polarized macrophages to reverse the immunosuppressive tumor microenvironment *in situ*. In multiple murine tumor models, the hydrogel adjuvant suppresses tumor growth, increases animal survival and long-term immunological memory, and protects mice against tumor rechallenge, leading to effective prophylactic and therapeutic responses. This work provides a potential chemical strategy to overcome the limitations associated with immunotherapy.



INTRODUCTION

Despite the successful removal of the visible tumor after surgical resection, patients still face a high risk of recurrence because of the microscopic residual disease left behind. Adjuvant therapies, such as immunotherapy, targeted therapy, and chemotherapy, are commonly employed to reduce the risk of tumor relapse by stimulating antitumor T cell responses to eliminate residual cancer cells.^{1,2} Although the current immunotherapy, specifically immune checkpoint blockade (ICB) treatment, has revolutionized cancer treatment, only a fraction of patients respond positively to immunotherapy alone. The immunosuppressive tumor microenvironment (TME) is partly responsible for the modest therapeutic responses.^{3,4} Furthermore, immunotherapy treatments are often administered systemically, giving rise to the potential for off-target effects and immune-related adverse effects. The ongoing research focuses on improving their targeting specificity, reducing immune-related side effects, and optimizing the balance between efficacy and safety.^{5–13} However, the tumor rejection responses induced by immunotherapy still need to be precisely controlled to amplify the immune responses within the TME and minimize the immune-related adverse effects.¹⁴

T cells play a crucial role in immunotherapy by recognizing and killing tumor cells. One of the killing mechanisms of T cells is the release of granzyme B (GrB), an aspartyl serine

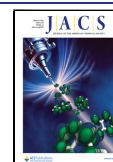
protease located in the cytotoxic granules of cytotoxic T lymphocytes (CTLs), natural killer (NK) cells, and lymphokine-activated killer cells. The cytotoxic GrB is liberated following the cell recognition-based conjugation with target cells, leading to apoptosis through caspase activation.¹⁵ Several probes have been reported to visualize the activity of GrB *in situ*, serving as assessing tools for immunotherapeutic responses.^{16–21} Despite the significance of GrB in immunotherapy, its secretion and activity differ depending on the specific therapy and individual patients because of the presence of an immunosuppressive TME and immunotherapy resistance. This variability will impact the therapeutic efficacy of immunotherapies significantly.^{22,23} Thus, developing a GrB-responsive immunotherapy represents a precise strategy for minimizing immune-related side effects while maximizing the effectiveness of immunotherapy by augmenting the secretion of GrB, thereby potentially overcoming the limitations observed in immunotherapy.

Received: January 12, 2024

Revised: February 26, 2024

Accepted: February 27, 2024

Published: March 13, 2024



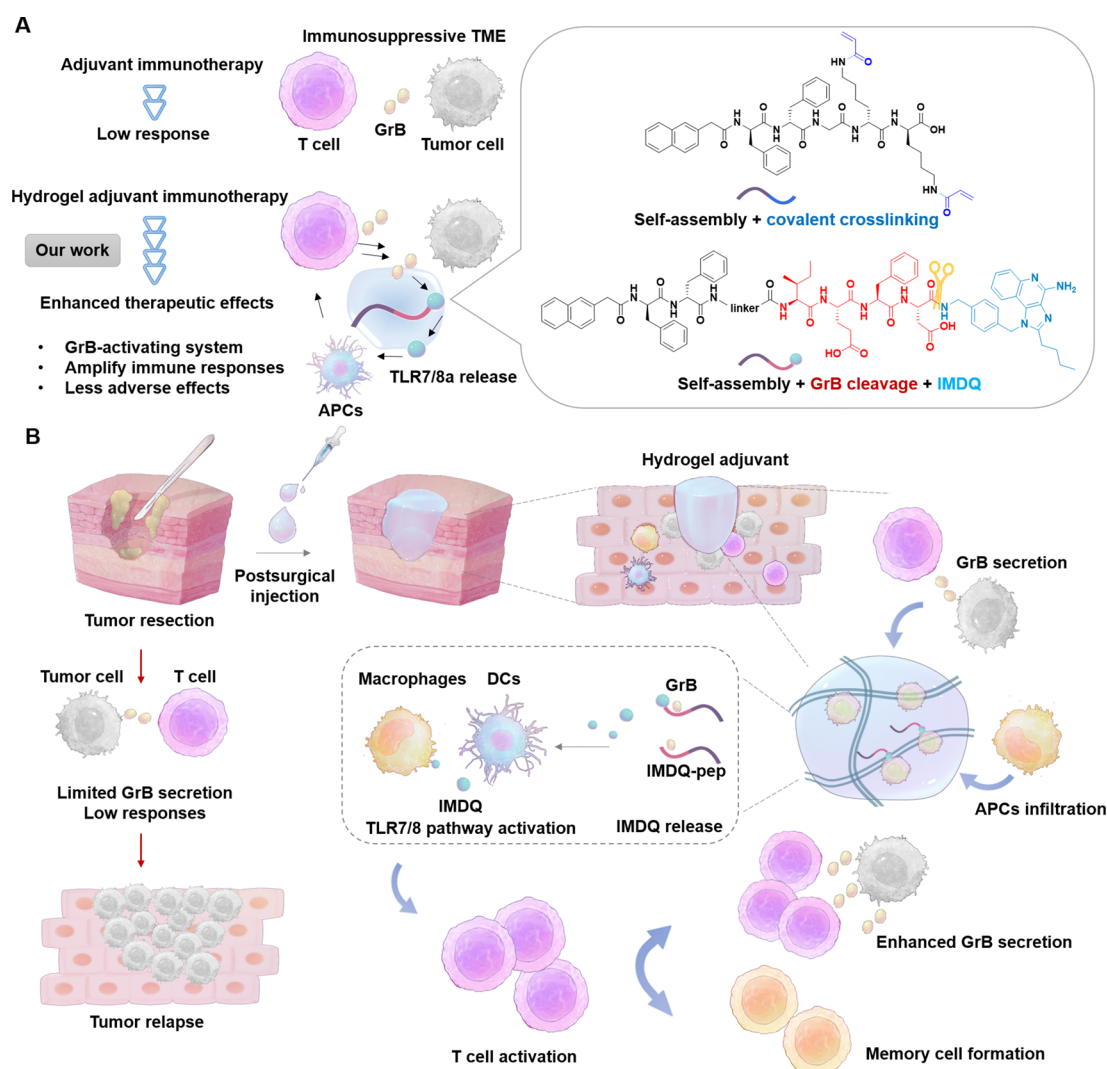


Figure 1. Composition of hydrogel adjuvant and the schematic mechanism for adjuvant-mediated postsurgical immunotherapy. (A) The structure of peptide scaffold and GrB responsive IMDQ-peptide conjugate. (B) By filling the surgical cavity with the hydrogel, it creates a localized inflammatory depot for infiltration of APCs. The localized release of IMDQ responds to GrB allowing for immune activation while minimizing immune-related toxicity, which are crucial for further enhancing GrB secretion and establishment of long-term immunological memory to improve personalized postsurgical immunotherapy.

Toll-like receptor (TLR) agonists are potent immune stimulators of antigen-presenting cells (APCs) that have shown great potential as adjuvants for cancer immunotherapy. Among the family of TLRs, TLR7/8 is broadly expressed on dendritic cells (DCs) and other APCs.²⁴ Imidazoquinoline (IMDQ) compounds, such as imiquimod and resiquimod (R848), have been found to activate TLR7/8, and their efficacy in gel and cream formulations has been evaluated in clinical trials.²⁵ However, TLR7/8 agonists can only be used for topical treatment because of quick elimination and systemic inflammation side effects. Recent efforts have been made to deliver TLR7/8 agonists through physical entrapment and TLR7/8 agonist-conjugated nanocarriers.^{26–33} Nonetheless, effectively triggering the release of TLR7/8 agonists to their free form at the disease site remains a challenge.³¹

This work describes a peptidic hydrogel adjuvant that responds intelligently to GrB to achieve enhanced and personalized postsurgical immunotherapy by filling the hydrogel into the cavity (Figure 1). We employed a GrB-cleavable isoleucine–glutamic acid–phenylalanine–aspartic acid (IEFD)

linkage to connect the IMDQ at the C-terminal of the self-assembling backbone.³⁴ This strategy addresses the limited secretion of GrB during immunotherapy by releasing the immunomodulator into its free form, activating the immune response, and further enhancing GrB secretion, while minimizing immune-related side toxicity. The resultant IMDQ-peptide conjugate and peptide scaffold could self-assemble into the fibrous network and further undergo photo-cross-linking to form a hydrogel, delivering tumor cells undergoing immunogenic cell death (ICD). The hydrogel adjuvant creates a localized inflammatory depot, facilitating the infiltration of DCs and macrophages. The adjuvant properties of the hydrogel allow for the local delivery of immunomodulators and danger signals along with tumor antigens to modulate immune responses, ultimately leading to the establishment of durable immunity and the generation of effective prophylactic responses. Furthermore, using this GrB-activating system after surgical resection, the hydrogel adjuvant could respond to the limited levels of GrB in the TME and release IMDQ. The localized release of free IMDQ effectively

reprograms the immunosuppressive TME and further boosts the immune responses against tumor cells. This targeted activation amplifies the immune responses specifically at the disease site, thus, reducing the potential for adverse effects in healthy tissues.

RESULTS AND DISCUSSION

Characterization of Covalently Self-Assembled Peptide Hydrogels. The short peptide-based hydrogels have attracted growing attention in recent years, because they are cost-effective, simple to prepare, and amenable for large scale.^{35–38} Several hybrid systems combining covalent and physical cross-linking have recently been developed, providing functional platforms for molecular delivery.^{39–41} Herein, we designed a short peptide, **NapffGk(aa)k(aa)** (Scheme S1), where **Napff** represents the *D*-configuration self-assembled block naphthalene–phenylalanine–phenylalanine that provides the noncovalent interactions such as hydrogen bonding and aromatic–aromatic interactions. The peptide also contains cross-linking monomers, denoted as **aa**, which can generate covalent bonds through photoinduced cross-linking with neighboring vinyl groups (Figure 1A). The use of *D*-amino acid in self-assembling peptide hydrogels has been reported to facilitate immunological outcomes and long-term antigen-presentation compared to those of their enantiomeric counterparts. This possible reason is the prolonged antigen persistence, reduced proteolytic susceptibility, and enhanced immune cell recruitment.⁴² This study selected acrylic acid (abbreviated as **aa**), which has been commercially used to modify natural and synthetic polymers for applications in tissue engineering and regenerative medicine, as a covalent bond-forming unit.⁴³ The peptide backbone is synthesized by a standard Fmoc-based solid-phase peptide synthesis (SPPS). The **aa** is conjugated to the lysine (K) of peptides by amide bond condensation. For comparison, the **NapffGkk** peptide is synthesized without the modification of **aa**. We also synthesized **NapGGGk(aa)k(aa)** peptide and **AcffGk(aa)k(aa)** peptide, where the phenylalanine–phenylalanine (**ff**) residues are substituted with glycine (G), and the Nap residue is replaced with an acetyl group (Ac). The purity and molecular weight of peptides are confirmed by liquid chromatography–mass (LC–MS, Figure S1 and Table S1) spectra and proton nuclear magnetic resonance (¹H NMR, Figures S2–S5). The GrB-responsive IMDQ-peptide conjugate **Napff-(PEG)₃-IEFD-IMDQ**, defined as **IMDQ-pep**, is synthesized via a condensation reaction. This reaction involves the amine group of IMDQ and the carboxyl group at the C-terminus of a peptide that contains the *D*-configuration self-assembled motif **Napff** and a poly(ethylene glycol) (PEG) chain. The *L*-configuration GrB-responsive linker, IEFD, is used to connect the two components (Scheme S2). The purity and molecular weight of peptides are confirmed by LC–MS spectra (Figure S6).

We first examined the gelation properties of peptide scaffolds. The lithium phenyl (2,4,6-trimethylbenzoyl) phosphinate (LAP) is employed as a photoinitiator due to its low toxicity, high solubility in water, and high reaction rate after irradiation.⁴⁴ After exposure to ultraviolet (UV) light ($\lambda = 365$ nm), only the **NapffGk(aa)k(aa)** peptide possesses the necessary properties for gel formation among the tested peptides. The other peptides fail to form hydrogels because of a loss of cross-links and aromatic–aromatic interactions (Figure S7). Thus, the **NapffGk(aa)k(aa)** peptide is selected

for the following characterization and subsequent biological experiments.

LC–MS result indicates a reduction in the remaining **NapffGk(aa)k(aa)** peptide with increasing irradiation time (Figure 2A). After 10 min of irradiation, the solution (10.0

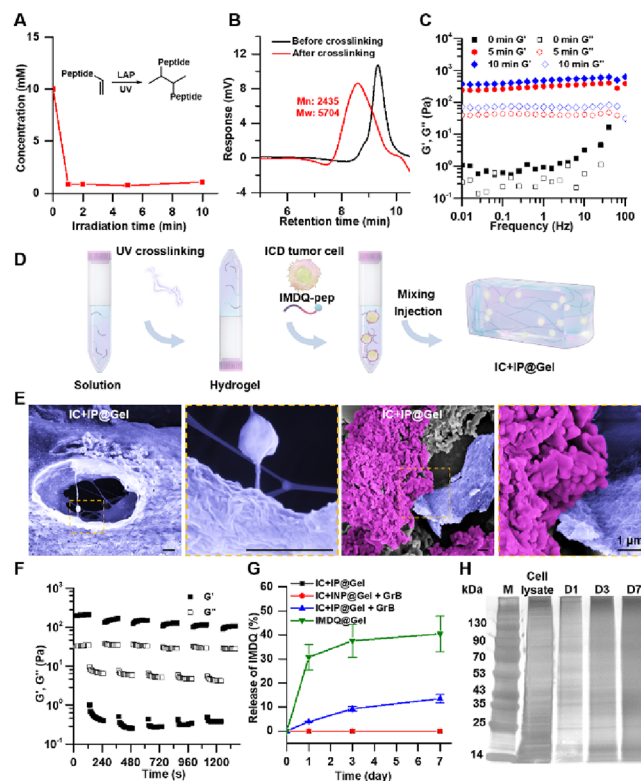


Figure 2. Characterization of covalently self-assembled peptide hydrogels and a hydrogel adjuvant. (A) The remaining **NapffGk(aa)k(aa)** peptide after irradiation is monitored by LC–MS. A solution of peptide (10 mM) is irradiated with UV light ($\lambda = 365$ nm) in the presence of LAP. (B) GPC spectra of **NapffGk(aa)k(aa)** peptide (10 mM) before and after photo-cross-linking. (C) Time-dependent rheological experiments of **NapffGk(aa)k(aa)** peptide (10 mM) after the irradiation. (D) The process for the production of **IC + IP@Gel**. (E) SEM images of **IC + IP@Gel**. Purple, ICD cells; blue, nanofibers formed by peptides. Scale bar: 1 μ m. (F) The shear-recovery measurement of **IC + IP@Gel**. (G) The release of **IMDQ-pep** in the presence and absence of GrB (50 μ g/mL) was tested by HPLC. (H) The SDS-PAGE analysis of released antigens from **IC + IP@Gel**.

mM) contains some peptide monomers with a conversion rate of 89.1%. To estimate the molecular weight of **NapffGk(aa)k(aa)** peptide after cross-linking, gel permeation chromatography (GPC) is performed. The peak shifts to a shorter retention time after the reaction, indicating the presence of a higher molecular weight product ($M_n = 2435$ Da and $M_w = 5704$ Da) compared with the peptide monomers (Figure 2B). Additionally, rheological transition during photoinduced gelation of peptides is investigated. The peptide easily dissolves in an aqueous solution and fails to form hydrogel prior to the formation of a covalent bond. The value of the G' surpasses the G'' after 10 min of irradiation, indicating the conversion from liquid to a hydrogel state (Figure 2C). These results demonstrate the successful formation of covalent bonds within the **NapffGk(aa)k(aa)** peptide hydrogel after UV irradiation and the vital roles of both covalent and noncovalent interactions in the gelation process.

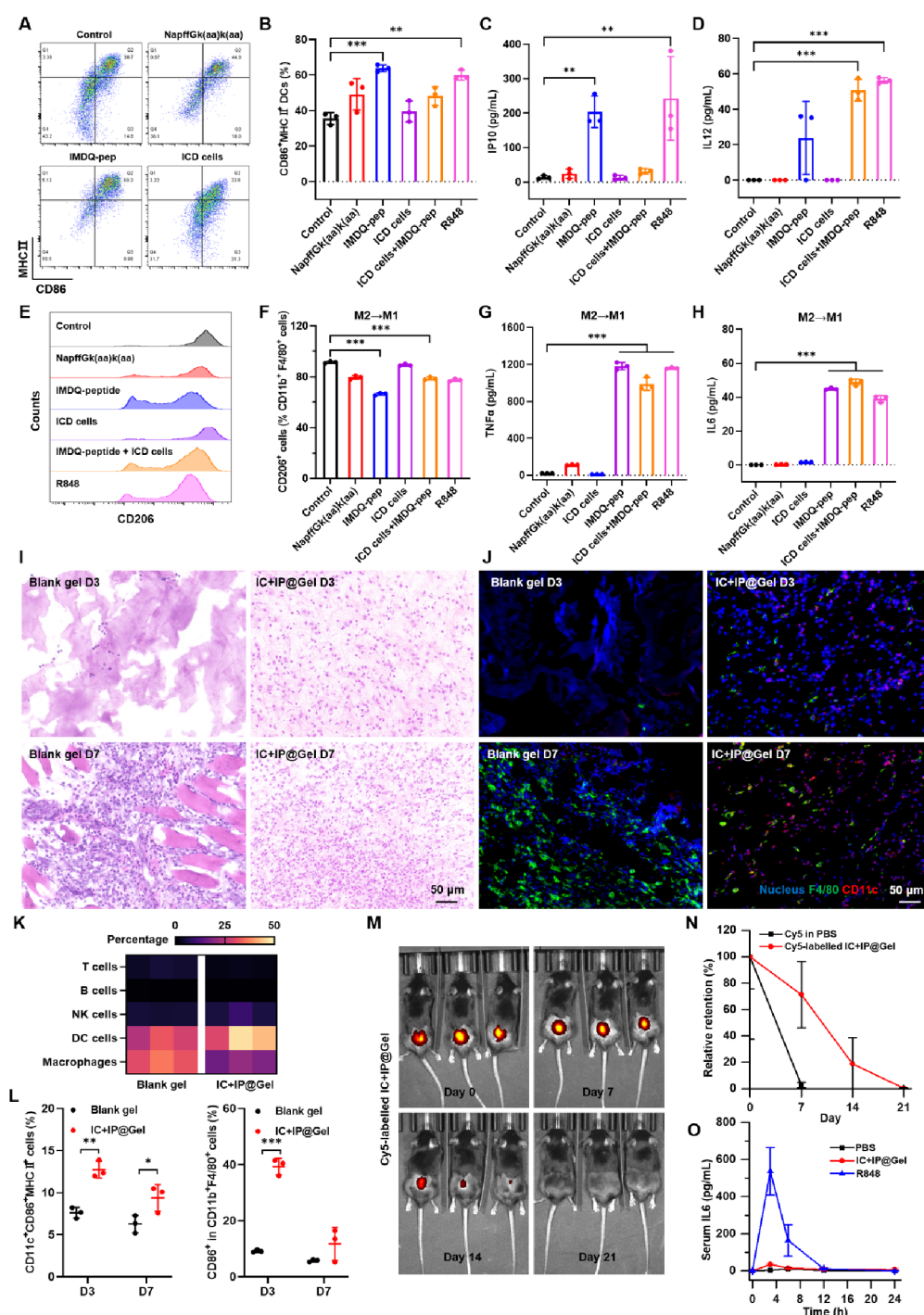


Figure 3. Immune-activating efficacy of hydrogel adjuvant *in vitro* and *in vivo*. (A) Representative FCM analysis of CD86⁺MHCII⁺ DCs and (B) the corresponding quantitative results. Production of IP10 (C) and IL12 cytokines (D) in the supernatants via ELISA. (E) Representative FCM analysis of CD206⁺ macrophages and (F) corresponding quantitative results for IL4-conditioned BMDMs. Production of TNF α (G) and IL6 cytokines (H) in the supernatants via ELISA. BMDCs and BMDMs were incubated with NapffGk(aa)k(aa) peptide (100 μ M), IMDQ-pep (10 μ M), ICD cells (10^5 cells), and the mixture of IMDQ-pep (10 μ M) and ICD cells for 12 h. (I) H&E staining of blank gel and IC + IP@Gel. (J) IF staining images of F4/80⁺ and CD11c⁺ cells in blank gel and IC + IP@Gel over 3 and 7 days after injection. Scale bar: 50 μ m. (K) Proportion of infiltrated T cells (CD3⁺), macrophages (F4/80⁺), B cells (CD19⁺), NK cells (NK1.1⁺), and DCs (CD11c⁺) in blank gel and IC + IP@Gel over 7 days after injection ($n = 3$) that is determined using FCM. (L) Quantitative analysis of infiltrated CD86⁺MHCII⁺ DCs and CD86⁺ macrophages by FCM over 7 days after injection ($n = 3$). (M) Fluorescence images of mice ($n = 3$) after Cy5-labeled IC + IP@Gel treatment and (N) relative retention of free Cy5 and Cy5-labeled IC + IP@Gel in mice. (O) Serum levels ($n = 3$) of IL6 over time following *s.c.* injection of PBS, IC + IP@Gel, and free R848. Data are depicted as mean \pm SD. Statistical significance is calculated using one-way ANOVA analysis. * $p < 0.05$, ** $p < 0.005$, and *** $p < 0.0005$.

The transmission electron microscopy (TEM) images reveal the formation of left-handed nanobelts with a diameter of ~ 20

nm in the sample of NapffGk(aa)k(aa) peptide, which transforms into nanofibers with larger width after photo-

cross-linking, indicating the morphology transitions of assemblies after covalent bond formation. The **IMDQ-pep** self-assembles into short nanofibers (Figure S8). Circular dichroism (CD) spectra show that the **NapffGk(aa)k(aa)** peptide exhibits characteristic signals near 200 and 220 nm (Figure S9). No noticeable changes in the CD signals upon irradiation of the peptide are observed. The Fourier transform infrared (FTIR) spectra indicate that the $\text{C}=\text{C}$ group of acrylic acids at the wavelength of 1000 cm^{-1} is lost, suggesting that the double bonds are fractured after the UV irradiation.⁴⁵ The peptide exhibits a stretching band at approximately 1634 cm^{-1} , indicating a β -sheet structure. The irradiated peptide retains its secondary structure consistent with original peptide.⁴⁶

Characterization of IC + IP@Gel Adjuvant. The hydrogel adjuvant, referred to as **IC + IP@Gel**, is obtained by mixing the hydrogel formed by the **NapffGk(aa)k(aa)** peptide with **IMDQ-pep** and tumor cells undergoing ICD (Figure 2D). The scanning electron microscope (SEM) images illustrate the formation of multiporous structures at the macroscale through the nanofibers and the dispersion of cells within the gel matrix, which enables the diffusion of antigens through the gel and their interactions with immune cells (Figure 2E). Moreover, the shear-recovery measurement demonstrates that the hydrogel exhibits high shear-thinning under high strain (100%) and rapid recovery upon strain reduction (1%), indicating that **IC + IP@Gel** possesses desirable injectable properties (Figure 2F).

The **IC + IP@Gel** is designed to maintain abundant antigens and present payloads sustainably for interaction with the surrounding cells. A GrB-cleavable linker is incorporated to achieve localized release of **IMDQ-pep** into its free form. The solubility of **IMDQ-pep** and its cumulative release are higher than those of the **Napff-PEG₃-IEFD-IMDQ** peptide (one PEG₃ chain as a linker, Figures S10 and S11), we thus retained two PEG₃ chains as the C-terminal modification of the self-assembled sequence. The cleavage rate and specificity are studied using high performance liquid chromatography (HPLC). The **IMDQ-pep** shows high specificity toward GrB with a maximum reaction rate (V_{max}) value of $1.19\text{ }\mu\text{M}/\text{min}$ and a Michaelis–Menten constant (K_{m}) value of $57.2\text{ }\mu\text{M}$ (Figure S12A), and it exhibits minimal response to other enzymes, including trypsin and cathepsin B (CTSB, Figure S12B). For comparison, an enzyme-nonresponsive **IMDQ-pep** conjugate **Napff-(PEG₃)₂-EIDF-IMDQ** is synthesized to create **IC + INP@Gel**, in which **IMDQ** is conjugated to the peptide backbone via a scrambled linker, **EIDF** (Figure S13). An *in vitro* release study was conducted to investigate the release of antigens and **IMDQ** from these formulations. The samples are incubated with phosphate-buffered saline buffer (PBS) at $37\text{ }^{\circ}\text{C}$ in the absence and presence of GrB, and the release of **IMDQ** and antigens are monitored over time using HPLC and sodium dodecyl sulfate-polyacrylamide gel electrophoresis (SDS-PAGE) analysis, respectively. The **IC + IP@Gel** shows a controllable release of **IMDQ** compared to other groups, and the release profile fits well to the first-order model (Figure S14A). The release of **IMDQ** from **IC + INP@Gel** barely increases in the presence of GrB. The cumulative release of **IMDQ** from **IC + IP@Gel** in the presence of GrB reaches approximately 15% after incubation for 7 days. In contrast, the free **IMDQ** encapsulated in the hydrogel (**IMDQ@Gel**) exhibits higher but uncontrolled burst release, indicating the potential immune-related side effects (Figure 2G). Corre-

spondingly, SDS-PAGE analysis (Figure 2H) and quantitative results (Figure S14B) indicate that the antigens are released in a continuous and controllable manner from the **IC + IP@Gel**, and the profile follows the first-order model. These results demonstrate the ability of the **IC + IP@Gel** to achieve a controlled and sustained release of **IMDQ** and antigens, which is desirable for their interactions with immune cells to promote the therapeutic efficacy of the adjuvant system and minimize potential side effects.⁴⁷

Immune-Activating Efficacy In Vitro. No significant differences in cytotoxicity or inhibition of cell proliferation are found against the normal human marrow stromal HS-5 cell line, indicating that the **NapffGk(aa)k(aa)** peptide could be applied to elicit the immune responses without raising significant concerns for cytotoxicity (Figure S15).

The APCs, including macrophages and DCs, are employed to investigate the immune-activating efficacy *in vitro*. Initially, murine bone marrow derived DCs (BMDCs) are exposed to the **NapffGk(aa)k(aa)** peptide, **IMDQ-pep**, and ICD cells. The expression of CD86 and MHCII and the secretion of cytokines are analyzed to assess the maturation and activation of BMDCs. The flow cytometry (FCM, Figure S16) analysis shows that compared to the negative control, the cells cultured with **NapffGk(aa)k(aa)** peptide and ICD cells display higher expression of CD86 (Figure S17A), which is a costimulatory molecule that plays a crucial role in T-cell activation.^{48,49} However, the treatment of **NapffGk(aa)k(aa)** peptide and ICD cells exhibit a lack of significant influence on the expression of MHCII (Figure S17B). The frequency of CD86⁺MHCII⁺ BMDCs treated with **NapffGk(aa)k(aa)** peptide and ICD cells has no obvious change compared to the negative control. In contrast, 60% of BMDCs treated with **IMDQ-pep** is double-positively stained with CD86 and MHCII, similar to the R848 positive control (Figure 3A,B). Additionally, the secretion of cytokines, including interferon-inducible protein-10 (IP10) and interleukin-12 (IL12), is significantly increased following **IMDQ-pep** treatment (Figure 3C,D). These cytokines are known to contribute to the chemoattraction of T cells, as well as augmented cytotoxicity of T cells and NK cells.^{50,51} The results indicate that the **IMDQ-pep** treatment triggers the upregulation of costimulatory molecule and MHCII molecules, along with the secretion of cytokines associated with immune cell activation. The combination of **IMDQ-pep** and ICD cells treatment further upregulates the CD86 expression but fails to affect the population of CD86⁺MHCII⁺ BMDCs significantly and the secretion of IP10. The expression of MHCII and IP10 could be regulated by interferon γ (IFN γ),^{50,52,53} which is primarily produced by activated immune cells. The counteracting effect on the frequency of CD86⁺MHCII⁺ DCs and induction of IP10 in DCs could be partly attributed to the interactions between IFN γ and its receptor expressed in tumor cells,⁵⁴ as evidenced by the limited IFN γ level in the supernatant (Figure S17C).

Furthermore, murine bone-marrow-derived macrophages (BMDMs) are incubated with hydrogel adjuvant components to investigate their polarization capacity. The FCM results indicate that the **IMDQ-pep** treatment induces the expression of CD86 (M1-related markers), suggesting the transformation of macrophages from an M0- to an M1-phenotype (Figures S18 and S19A). Enzyme-linked immunosorbent assay (ELISA) measurements of protein levels reveal that the **IMDQ-pep** treatment results in higher levels of secretion of tumor necrosis

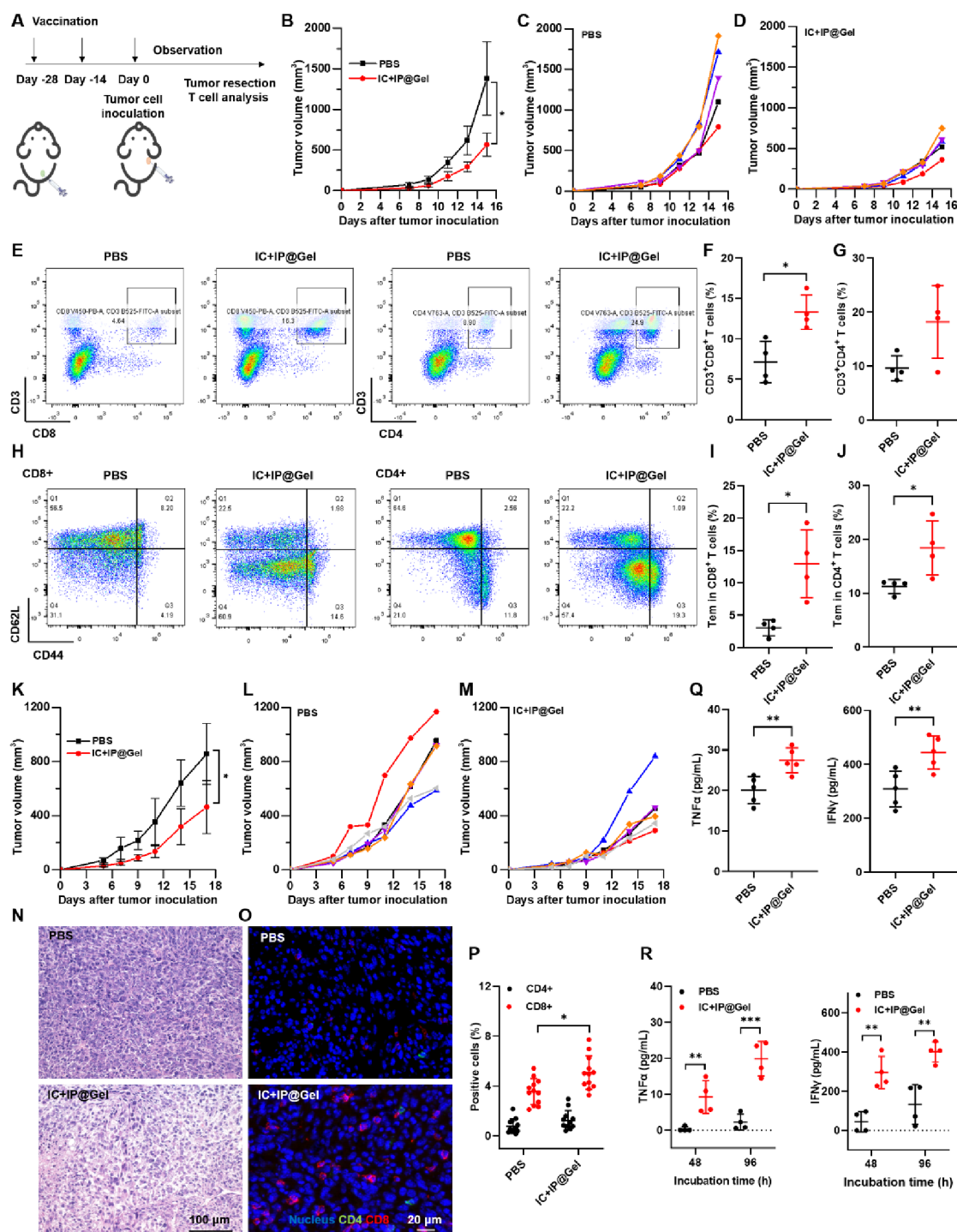


Figure 4. IC + IP@Gel vaccination induces prophylactic efficacy against B16F10 and MC38 tumors. (A) Schedule for vaccination, tumor inoculation, and the prophylactic immune response test. (B) The average B16F10 tumor growth curves ($n = 5$). (C and D) The tumor growth curves of individual animals. (E) Representative FCM analysis of $CD3^+CD8^+$ and $CD3^+CD4^+$ T cells in tumors at day 15 and (F and G) corresponding quantitative results. (H) Representative FCM plots of Tem cells ($CD44^+CD62L^-$) in the spleens at day 15 and (I and J) corresponding quantitative results. (K) The average MC38 tumor growth curves ($n = 6$). (L and M) The tumor growth curves of individual animals. (N) H&E staining of tumors. Scale bar: 100 μm . (O) IF staining images and (P) quantitative analysis of infiltrated $CD4^+$ and $CD8^+$ T cells in tumors. Scale bar, 20 μm . (Q) Production of $\text{TNF}\alpha$ and $\text{IFN}\gamma$ cytokines in tumors. (R) Production of $\text{TNF}\alpha$ and $\text{IFN}\gamma$ cytokines related to the antigen-specific response in the spleens. Data are depicted as mean \pm SD. Statistical significance is calculated using Student's t test analysis. * $p < 0.05$, ** $p < 0.005$, and *** $p < 0.0005$.

factor α ($\text{TNF}\alpha$) and interleukin-6 (IL6) compared to the control group (Figure S19B,C). This result indicates that **IMDQ-pep** can elicit the production of proinflammatory cytokines by macrophages. The repolarization of M2-like

macrophages to M1 phenotype is also evaluated in interleukin-4 (IL4)-conditioned BMDMs, which express typical M2-like macrophage marker CD206.^{55–57} Compared to the control group, treatment with **IMDQ-pep** significantly decreases the

expression of CD206 (Figure 3E, F). As expected, IMDQ-pep treatment stimulates the production of proinflammatory cytokines, as evidenced by the evaluated levels of TNF α and IL6 in the supernatants. In contrast, the NapffGk(aa)k(aa) peptide alone and ICD cells minimally induce the production of cytokines (Figure 3G,H). These findings demonstrate the efficacy of the hydrogel adjuvant components in stimulating the maturation of DCs, the expression of M1-related markers, and the secretion of proinflammatory cytokine. This result indicates the potential of these components as immunomodulatory agents in antitumor therapies.

Immune Cell Infiltration, Degradation, and Toxicity of IC + IP@Gel *In Vivo*. We next evaluated the immune responses of the IC + IP@Gel adjuvant *in vivo*. We immunized C57BL/6J mice subcutaneously (*s.c.*) at the tail base with a single dose of the hydrogel adjuvant. On day 3 and day 7 postimmunization, the gel is collected for hematoxylin and eosin (H&E) staining, immunofluorescence (IF) staining, and FCM analysis. Results from H&E and IF staining show that the blank gel itself induces the infiltration of macrophages toward the scaffold on day 7, compared to that on day 3, when only the gel scaffold is observed. However, IC + IP@Gel results in a rapid influx of DCs and macrophages over time (Figure 3L,J). Meanwhile, the FCM analysis of the gel scaffold collected on day 7 postimplantation confirms the infiltration of immune cells (CD45⁺), including DCs, macrophages, T cells, B cells, and NK cells (Figures S20 and 3K). Moreover, the IC + IP@Gel significantly increases the percentage of activated DCs and M1-phenotype macrophages, a critical step in antigen presentation and subsequent stimulation of tumor-specific immunity.⁵⁸ Whereas vaccination with blank gel alone results in minimal induction of DC maturation and macrophage M1 polarization (Figure 3L). These results demonstrate the potency of the IC + IP@Gel to recruit and generate antitumor immune responses *in vivo*.⁵⁹

Given that a large number of macrophages are observed in the injected gel, the gel is supposed to be gradually engulfed by phagocytes. The Cy5-labeled IC + IP@Gel is prepared for the visualization and tracking of the gel *in vivo* (Figure S21 and Scheme S3). Fluorescence images of mice indicate that the Cy5-labeled IC + IP@Gel exhibits a relatively slight decrease within the first 7 days, eventually disappearing entirely after approximately 21 days, which suggests its excellent biodegradability and biocompatibility (Figure 3M,N). The local injection of the free R848 drug leads to a high level of serum IL6, indicating the potential for systemic toxicity and side effects. In contrast, treating IC + IP@Gel minimizes the systemic cytokine, indicating the safety of hydrogel adjuvant (Figure 3O). The chemical conjugation of IMDQ onto the peptide is responsible for localized release and stimulation, contributing to a decrease in immune-related adverse events.

Prophylactic Efficacy of IC + IP@Gel *In Vivo*. Healthy C57BL/6J mice are implanted *s.c.* with IC + IP@Gel containing ICD B16F10 cells twice before tumor inoculation (Figure 4A). The effects of vaccination on tumor progression, body weight, and immune responses are evaluated. Compared with the PBS group, vaccination with IC + IP@Gel slows the tumor progression (Figure 4B–D). The body weight of all mice was not reduced throughout the experimental period, indicating that the vaccination could not cause significant adverse effects (Figure S22). The immune mechanism underlying the antitumor effects is analyzed using FCM on day 15 (Figures S23 and 4E). The proportion of CTLs (CD8⁺)

within the tumors increases markedly (1.86-fold increase) after IC + IP@Gel vaccination compared to the PBS group (Figure 4F). Additionally, a higher frequency of infiltrated CD4⁺ T cells (1.89-fold increase) is observed (Figure 4G), indicating that IC + IP@Gel induces efficient antitumor immunity. To investigate the immune memory effect of the hydrogel adjuvant, splenocytes in a single-cell suspension are collected and analyzed using FCM (Figures S24 and 4H). The IC + IP@Gel vaccination expands the population of splenic CD8⁺ and CD4⁺ effector memory T (Tem) cells (4.23-fold increase and 1.64-fold increase, respectively). In contrast, such effects from the PBS group are limited (Figure 4I,J). The vaccination significantly expands splenic Tem cells, indicating the establishment of a durable immunity.

We further evaluated the prophylactic efficacy in a highly immunogenic MC38 tumor model to demonstrate its broad application. The IC + IP@Gel treated mice exhibit a significant delay of tumor growth, with a tumor inhibition rate of 40.2% (Figures 4K–M and S25). Throughout the experimental period, there is no observable body weight loss (Figure S26). A H&E analysis of the tumor section is conducted to verify the prophylactic effect. The tumor cells in the PBS group display typical morphologies, with no visible apoptotic cells. In contrast, tumors treated with IC + IP@Gel have extensively specific changes, such as apoptotic cells marked by cell shrinkage and nuclear condensation, and necrotic cells characterized by their pink cytoplasm with vanished nuclei (Figure 4N). The IC + IP@Gel vaccination results in a 1.43-fold and 1.58-fold higher fraction of infiltrating CD8⁺ and CD4⁺ T cells, respectively (Figure 4O,P). Additionally, it enhances the secretion of TNF α (1.37-fold increase) and IFN γ (1.44-fold increase) within the tumors compared to the PBS group, suggesting enhanced antitumor immunity (Figure 4Q). Although the vaccination can enhance the antitumor T cell responses, the presence of high levels of intratumoral programmed cell death 1 ligand 1 (PD-L1) counteracts these immune responses (Figure S27), contributing to the failure of complete tumor prevention. The IC + IP@Gel vaccination leads to an expansion of CD8⁺ central memory T cells (Tcm, 1.17-fold increase) and CD4⁺ Tem cells (1.20-fold increase) compared to the PBS group (Figure S28). Given the antitumor T cell responses mediated by both Tcm and Tem subsets, we isolated the splenocytes to evaluate the antigen-specific memory. After restimulating with MC38 cell lysis *in vitro*, mice treated with IC + IP@Gel produce higher levels of TNF α (24.78-fold increase and 8.88-fold increase after 48 and 96 h incubation, respectively) and IFN γ (6.68-fold increase and 3.02-fold increase after 48 and 96 h incubation, respectively) in relative to the PBS group (Figure 4R). This result suggests the establishment of protective T-cell immunity and a fast response to the tumor antigens. Together, these results offer critical evidence that IC + IP@Gel vaccination effectively suppresses tumor growth and generates memory immunity. The histology analysis of major organs shows no significant difference between IC + IP@Gel-treated mice and mice in the PBS group, suggesting that local treatment does not cause noticeable systemic adverse effects on the mice (Figure S29).

Therapeutic Efficacy in Postsurgical Tumor Recurrence Models. Having confirmed the prophylactic response of IC + IP@Gel after *in vivo* injection, where it could function as a therapeutic reservoir, we evaluated the synergistic antitumor effects of IC + IP@Gel by using tumor recurrence

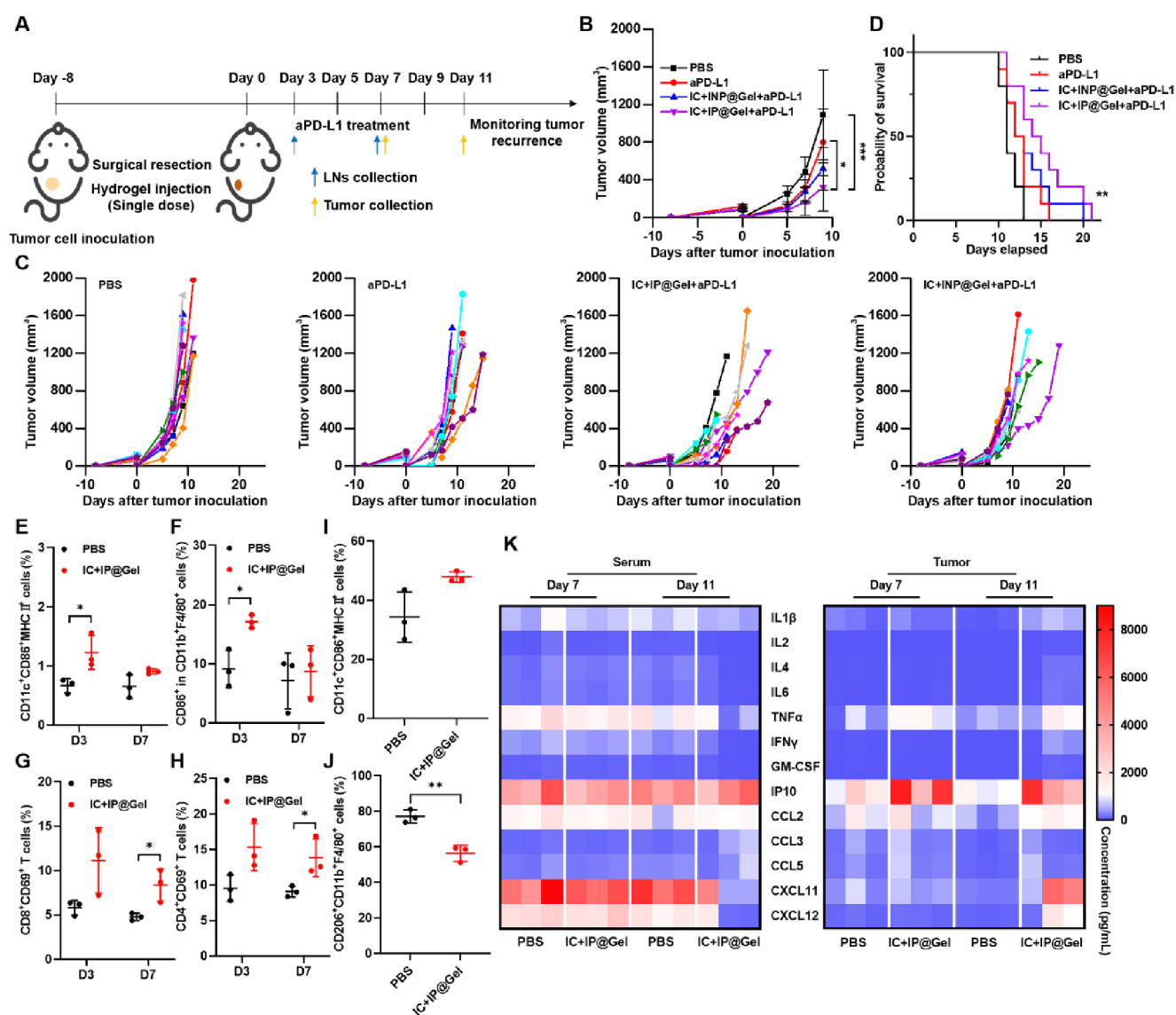


Figure 5. Antitumor effect on the postsurgical B16F10 model. (A) Schedule for tumor cell inoculation, surgical resection, hydrogel injection, immune response analysis, and antitumor effect evaluation. (B) The average tumor growth curves of mice ($n = 10$). (C) The tumor growth curves of individual animals. (D) The survival curves of mice in different groups. Quantification of activated DCs ($CD86^+MHCII^+CD11c^+$, E), M1 phenotype macrophages ($CD86^+$, F), activated $CD8^+$ T cells ($CD69^+$, G), and activated $CD4^+$ T cells ($CD69^+$, H) in lymph nodes on days 3 and 7 by FCM analysis. Quantification of activated DCs ($CD86^+MHCII^+CD11c^+$, I) and M2 phenotype macrophages ($CD206^+$, J) in tumors on day 11 by FCM analysis. (K) Cytokines and chemokines secreted in tumor and serum of mice. Data are depicted as mean \pm SD. Statistical significance is calculated using Student's t test and one-way ANOVA analysis. Differences in survival are determined using the Kaplan–Meier method, and the overall p value is calculated by the log-rank test. * $p < 0.05$, ** $p < 0.005$, and *** $p < 0.0005$.

models. The B16F10 cells are injected *s.c.* into the back of the mice. On day 8 after inoculation, surgery is performed to remove approximately 90% of the primary tumor tissue. The resection space is then implanted with IC + IP@Gel. Following the surgery, mice are administered four doses of anti-PD-L1 antibody (Figure 5A). The mice did not experience any significant decrease in weight during the experiment, indicating that the treatments had no significant adverse effects (Figure S30). All mice in the PBS group suffer from substantial recurrent tumors and die within 13 days. Mice treated with anti-PD-L1 alone exhibit fast tumor recurrence. Treatment with IC + IP@Gel results in a 70.4% reduction in tumor volume, while the IC + INP@Gel group experiences a 52.6% reduction (Figure 5B,C). Furthermore, the administration of IC + IP@Gel extends the survival of animals, with a median

survival time of 14.5 days (Figure 5D). These results suggest that using IC + IP@Gel in the surgical area could significantly reduce tumor growth and improve survival outcomes.

Lymph nodes are collected and analyzed using FCM on days 3 and 7 after treatment to investigate the changes in immune responses in mice. On day 3, the treatment with IC + IP@Gel leads to a significant increase in the ratio of activated DCs (1.85-fold increase) and M1 phenotype macrophages (1.88-fold increase) over the PBS group (Figure 5E,F). These changes are essential for the cross-presentation and activation of T cells. Similar findings are observed for the early activated T cells. On day 7 after treatment, the IC + IP@Gel-treated mice maintain a sustained high proportion of activated $CD8^+$ T cells (1.75-fold increase) and activated $CD4^+$ T cells (1.52-fold increase) compared to the PBS group (Figure 5G,H). These

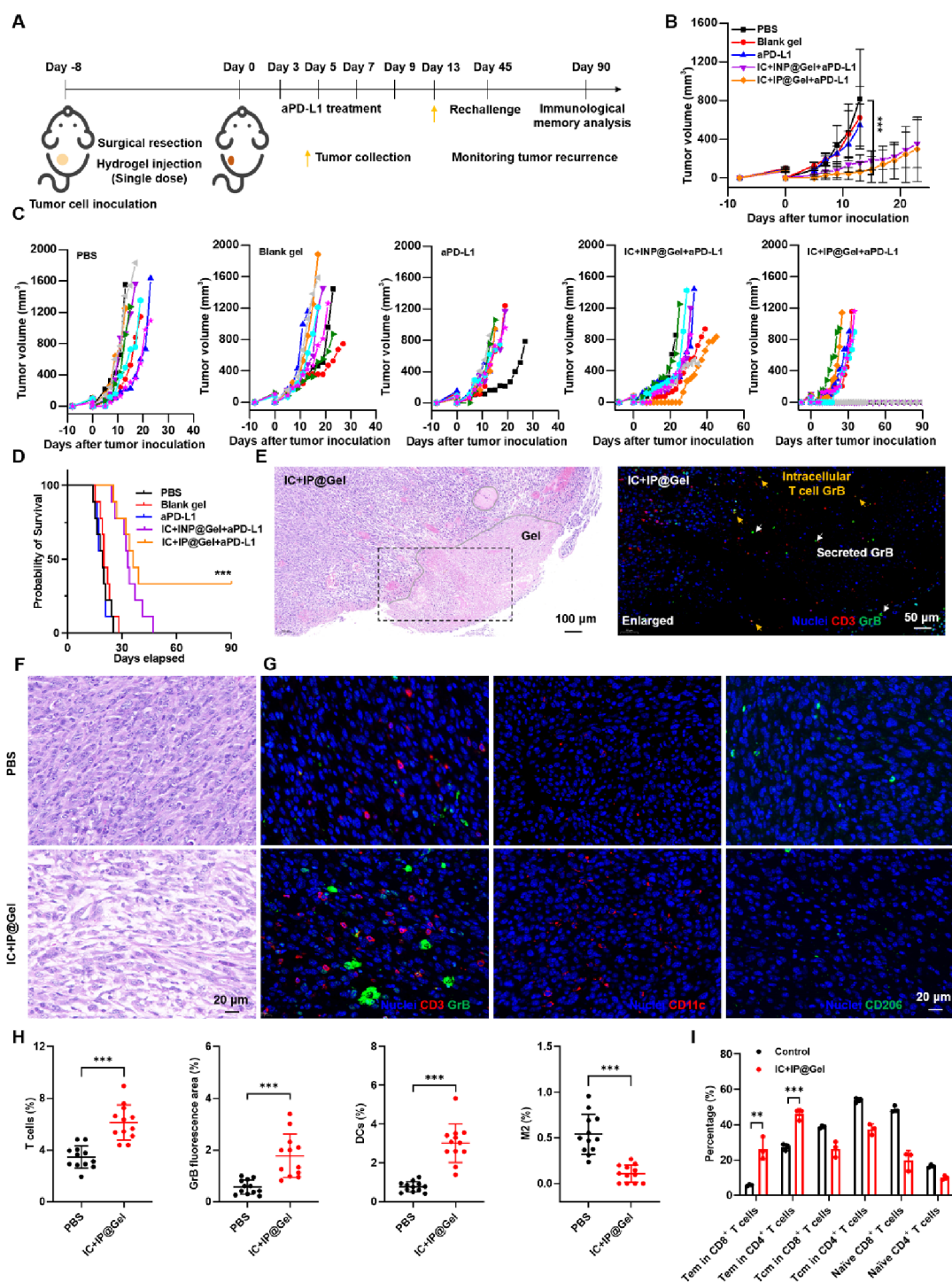


Figure 6. Antitumor effect on postsurgical MC38 model. (A) Schedule for tumor cell inoculation, surgical resection, hydrogel injection, immune response analysis, tumor rechallenge, and antitumor effect evaluation. (B) The average tumor growth curves of mice ($n = 9$). (C) The tumor growth curves of individual animals. (D) The survival curves of mice in different groups. (E) H&E staining and if staining images of hydrogel within the tumor. The dashed line represents the implanted gel. (F) H&E staining of tumors. Scale bar: 20 μ m. (G) IF staining images and (H) quantitative analysis of infiltrated T cells (CD3⁺), secretion of GrB, infiltrated DCs (CD11c⁺), and M2 phenotype macrophages (CD206⁺) in tumors on day 13. Scale bar: 20 μ m. (I) Quantitative analysis of Tem cells in the spleens on day 90 using FCM. Data are depicted as mean \pm SD. Statistical significance is calculated using Student's *t* test and one-way ANOVA analysis. Differences in survival are determined using the Kaplan–Meier method, and the overall *p* value is calculated by the log-rank test. **p* < 0.05, ***p* < 0.005, and ****p* < 0.0005.

results suggest a trafficking of DCs and T cells and a continued activation of T cells within the lymph nodes. The activity levels of immune cells within the tumors are analyzed using FCM on day 11 to profile the changes in the TME. The results show that intratumoral activated DCs remain 1.40-fold higher than

the PBS group (Figure S1), indicating the immune-activating effect of IC + IP@Gel. Additionally, there is a 26.9% decrease in the number of M2 phenotype macrophages after treatment with IC + IP@Gel (Figure S2). Furthermore, the secretion of cytokines and chemokines in serum and tumor is evaluated

using Luminex on days 7 and 11 (Figure 5K). Most cytokines and chemokines in the blood show no apparent changes after IC + IP@Gel injection. In tumoral tissues, the injection of IC + IP@Gel stimulates the production of TNF α (2.8-fold increase) and IP10 (3.6-fold increase) to exert antitumor activity 7 days post-treatment. Moreover, the concentrations of cytokines and chemokines such as IL6 (19.1-fold increase), TNF α (2.2-fold increase), IFN γ (50.8-fold increase), granulocyte-macrophage colony-stimulation factor (GM-CSF, 41.3-fold increase), IP10 (4.6-fold increase), CC-chemokine ligand 3 (CCL3, 2.6-fold increase), and C-X-C motif chemokine ligand 11 (CXCL11, 17.3-fold increase) further increase in the following 4 days. These factors contribute to inhibiting tumor angiogenesis and proliferation, the facilitation of immune cell migration, and the correct function of CD8⁺ T cells.^{50,60–62} These observations suggest that local implantation of IC + IP@Gel could reprogram the immunosuppressive TME and enhance the antitumor T cell responses while minimizing systemic toxicity.

The efficacy of IC + IP@Gel for the treatment of postsurgical tumor recurrence is also evaluated using the MC38 tumor model (Figure 6A). The body weights of mice are not affected by surgery or local treatments (Figure S31). All mice treated with PBS and blank gel developed fast tumor recurrence. Mice treated with anti-PD-L1 alone slow tumor growth but experience fast tumor recurrence during the treatment-free period. In contrast, mice receiving IC + IP@Gel and IC + INP@Gel show a greater ability to suppress tumor growth (Figure 6B,C) and prolong survival time (Figure 6D) in comparison to the other groups, indicating a potent ability of hydrogel adjuvant to resist tumor recurrence.

Due to the superior response of animals to IC + IP@Gel treatment compared to the PBS group, we analyzed the infiltration of immune cells using H&E and IF staining of tumor tissue on day 13. The remaining gel within the tumors could be observed in the H&E staining image. Following IC + IP@Gel treatment, IF images show the colocalization of GrB staining with regions of CD3⁺ staining, the release of GrB into the extracellular space, and its localization in the gel region (Figure 6E). This result is essential for the controlled release of IMDQ. The treatment with hydrogel adjuvant induces histological changes, including the appearance of apoptotic cells and necrotic cells (Figure 6F). Furthermore, the IF staining images demonstrate that IC + IP@Gel-treated tumors exhibit a higher number of infiltrated T cells (1.78-fold increase), enhanced secretion of GrB (3.13-fold increase), and a 3.93-fold increase in DC levels compared to the PBS group (Figure 6G,H). The treatment of IC + IP@Gel leads to a 2.28-fold increase in GrB secretion than the treatment with anti-PD-L1 alone (Figure S32). This result suggests enhanced cytotoxic activity of immune cells in the IC + IP@Gel-treated tumors. In addition, the percentage of the immunosuppressive M2 phenotype cells in the IC + IP@Gel-treated mice decrease by 80.1% relative to the PBS group (Figure 6G,H), indicating a positive association with the tumoricidal microenvironment.

Encouragingly, complete tumor rejection is observed in 33% of mice in the IC + IP@Gel group within 45 days, while continuous tumor recurrence occurs and all mice die within 47 days in the IC + INP@Gel group, suggesting that IC + IP@Gel is more effective in achieving long-term tumor suppression (Figure 6D). This observed outcome is probably associated with the release of immunomodulators from IC + IP@Gel. These immunomodulators have the potential to enhance the

penetration into the tumor, thereby promoting the activation and expansion of immune cells rather than limiting their activation within the hydrogel. Tumor-free mice are rechallenged with MC38 cells on the contralateral side of the primary tumors to assess the establishment of immune memory. After surveillance for another 45 days, no tumor recurrence could be found, indicating the establishment of long-term immunity against tumor recurrence after local injection of IC + IP@Gel. 90 days after treatment, the spleens and peripheral blood are collected and analyzed by using FCM to examine memory immune cells. In the spleens of IC + IP@Gel-treated mice, there is a significant increase in the percentages of CD4⁺ Tem (1.68-fold increase) and CD8⁺ Tem (4.61-fold increase) cells compared to the mice of the same age (Figure 6I). Meanwhile, mice injected with hydrogel adjuvant did not exhibit any obvious changes in the composition of immune cells in their blood (Figure S33), indicating that the local treatment has no effect on the immune cell population in the bloodstream.

These results collectively suggest that IC + IP@Gel treatment promotes a favorable immune environment characterized by increased DC activation and T cell infiltration, enhanced secretion of cytotoxic molecules like GrB, and reduced presence of immunosuppressive M2 phenotype cells. Moreover, IC + IP@Gel treatment also induces the generation of memory immune cells. These changes contribute to the establishment of a tumoricidal microenvironment that is favorable for inhibiting tumor growth, promoting antitumor immune responses, and ultimately leading to long-term tumor suppression.

CONCLUSION

In summary, this work describes a GrB-responsive adjuvant leveraging peptide-based hydrogel depot technology to improve the effectiveness of postsurgical immunotherapy. This system releases the immunomodulator into its free form in response to the limited secretion of GrB during immunotherapy. The hydrogel adjuvant activates the immune response and further enhances the secretion of GrB. This dual mechanism of action helps to amplify and expand the antitumor immune responses at disease sites, leading to an enhanced therapeutic effect and establishing long-term immunity while minimizing immune-related toxicity. The GrB-activating system provides an intelligent strategy for adjuvants to activate locally, thus improving the effectiveness and safety of immunotherapy.

ASSOCIATED CONTENT

Supporting Information

The Supporting Information is available free of charge at <https://pubs.acs.org/doi/10.1021/jacs.4c00569>.

Details on experimental procedures and additional characterization, including details of peptide synthesis and characterization, LC–MS spectra, NMR spectra, optical images of hydrogel, TEM images, CD and FTIR spectra, cytotoxicity of peptides, release profile of IMDQ and antigens, FCM results, IF staining images, body weight of mice, and H&E staining images (PDF)

AUTHOR INFORMATION

Corresponding Author

Huaimin Wang – Department of Chemistry, School of Science, Institute of Natural Sciences, Westlake Institute for Advanced Study, Westlake University, Hangzhou, Zhejiang 310024, China; Westlake Laboratory of Life Sciences and Biomedicine, Hangzhou, Zhejiang 310024, China; orcid.org/0000-0002-8796-0367; Email: wanghuaimin@westlake.edu.cn

Authors

Bihan Wu – Department of Chemistry, Zhejiang University, Hangzhou, Zhejiang 310058, China; Department of Chemistry, School of Science, Institute of Natural Sciences, Westlake Institute for Advanced Study, Westlake University, Hangzhou, Zhejiang 310024, China

Juan Liang – Department of Chemistry, School of Science, Institute of Natural Sciences, Westlake Institute for Advanced Study, Westlake University, Hangzhou, Zhejiang 310024, China

Xuejiao Yang – Department of Chemistry, School of Science, Institute of Natural Sciences, Westlake Institute for Advanced Study, Westlake University, Hangzhou, Zhejiang 310024, China

Yu Fang – Department of Chemistry, School of Science, Institute of Natural Sciences, Westlake Institute for Advanced Study, Westlake University, Hangzhou, Zhejiang 310024, China

Nan Kong – Department of Chemistry, School of Science, Institute of Natural Sciences, Westlake Institute for Advanced Study, Westlake University, Hangzhou, Zhejiang 310024, China

Dinghao Chen – Department of Chemistry, School of Science, Institute of Natural Sciences, Westlake Institute for Advanced Study, Westlake University, Hangzhou, Zhejiang 310024, China

Complete contact information is available at:

<https://pubs.acs.org/10.1021/jacs.4c00569>

Notes

The authors declare the following competing financial interest(s): The authors have applied for a patent on this strategy.

ACKNOWLEDGMENTS

This project was supported by the National Natural Science Foundation of China (82272145) and the Foundation of Westlake University. We thank the Instrumentation and Service Center for Molecular Sciences, Instrumentation and Service Center for Physical Sciences, General Equipment Core Facility, Biomedical Research Core Facilities, and Laboratory Animal Resource Center at Westlake University for the assistance with measurements.

REFERENCES

- (1) Burotto, M.; Wilkerson, J.; Stein, W. D.; Bates, S. E.; Fojo, T. Adjuvant and neoadjuvant cancer therapies: A historical review and a rational approach to understand outcomes. *Semin. Oncol.* **2019**, *46* (1), 83–99.
- (2) Patel, S. P.; Othus, M.; Chen, Y.; Wright, G. P.; Yost, K. J.; Hynstrom, J. R.; Hu-Lieskovan, S.; Lao, C. D.; Fecher, L. A.; Truong, T.-G.; et al. Neoadjuvant-adjuvant or adjuvant-only pembrolizumab in advanced melanoma. *N. Engl. J. Med.* **2023**, *388* (9), 813–823.
- (3) Havel, J. J.; Chowell, D.; Chan, T. A. The evolving landscape of biomarkers for checkpoint inhibitor immunotherapy. *Nat. Rev. Cancer* **2019**, *19* (3), 133–150.
- (4) Morad, G.; Helmink, B. A.; Sharma, P.; Wargo, J. A. Hallmarks of response, resistance, and toxicity to immune checkpoint blockade. *Cell* **2021**, *184* (21), 5309–5337.
- (5) Fan, Y. C.; Kuai, R.; Xup, Y.; Ochyl, L. J.; Irvine, D. J.; Moon, J. J. Immunogenic cell death amplified by co-localized adjuvant delivery for cancer immunotherapy. *Nano Lett.* **2017**, *17* (12), 7387–7393.
- (6) Ci, T. Y.; Li, H. J.; Chen, G. J.; Wang, Z. J.; Wang, J. Q.; Abdou, P.; Tu, Y. M.; Dotti, G.; Gu, Z. Cryo-shocked cancer cells for targeted drug delivery and vaccination. *Sci. Adv.* **2020**, *6* (50), No. eabc3013.
- (7) Zhang, J.; Chen, C.; Li, A. N.; Jing, W. Q.; Sun, P.; Huang, X. Y.; Liu, Y. C.; Zhang, S. C.; Du, W.; Zhang, R.; et al. Immunostimulant hydrogel for the inhibition of malignant glioma relapse post-resection. *Nat. Nanotechnol.* **2021**, *16* (5), 538–548.
- (8) Grosskopf, A. K.; Labanieh, L.; Klysz, D. D.; Roth, G. A.; Xu, P.; Adebowale, O.; Gale, E. C.; Jons, C. K.; Klich, J. H.; Yan, J.; et al. Delivery of CAR-T cells in a transient injectable stimulatory hydrogel niche improves treatment of solid tumors. *Sci. Adv.* **2022**, *8* (14), No. eabn8264.
- (9) Chen, C.; Jing, W. Q.; Chen, Y.; Wang, G. Y.; Abdalla, M.; Gao, L.; Han, M. S.; Shi, C. D.; Li, A. N.; Sun, P.; et al. Intracavity generation of glioma stem cell-specific CAR macrophages primes locoregional immunity for postoperative glioblastoma therapy. *Sci. Transl. Med.* **2022**, *14* (656), No. eabn1128.
- (10) Wang, F. H.; Huang, Q.; Su, H.; Sun, M. J.; Wang, Z. Y.; Chen, Z. Q.; Zheng, M. Z.; Chakroun, R. W.; Monroe, M. K.; Chen, D. Q.; et al. Self-assembling paclitaxel-mediated stimulation of tumor-associated macrophages for postoperative treatment of glioblastoma. *Proc. Natl. Acad. Sci. U. S. A.* **2023**, *120* (18), No. e2204621120.
- (11) Sun, M. Y.; Liu, Z. W.; Wu, L.; Yang, J.; Ren, J. S.; Qu, X. G. Bioorthogonal-activated in situ vaccine mediated by a COF-based catalytic platform for potent cancer immunotherapy. *J. Am. Chem. Soc.* **2023**, *145* (9), 5330–5341.
- (12) Gao, G.; Jiang, Y. W.; Zhan, W. J.; Liu, X. Y.; Tang, R. Q.; Sun, X. B.; Deng, Y.; Xu, L. L.; Liang, G. L. Trident molecule with nanobrush-nanoparticle-nanofiber transition property spatially suppresses tumor metastasis. *J. Am. Chem. Soc.* **2022**, *144* (26), 11897–11910.
- (13) Wang, F. H.; Su, H.; Xu, D. Q.; Dai, W. B.; Zhang, W. J.; Wang, Z. Y.; Anderson, C. F.; Zheng, M. Z.; Oh, R.; Wan, F. Y.; et al. Tumour sensitization via the extended intratumoural release of a STING agonist and camptothecin from a self-assembled hydrogel. *Nat. Biomed. Eng.* **2020**, *4* (11), 1090–1101.
- (14) Hu, Z.; Ott, P. A.; Wu, C. J. Towards personalized, tumour-specific, therapeutic vaccines for cancer. *Nat. Rev. Immunol.* **2018**, *18* (3), 168–182.
- (15) Hiebert, P. R.; Granville, D. J. Granzyme B in injury, inflammation, and repair. *Trends Mol. Med.* **2012**, *18* (12), 732–741.
- (16) Nguyen, A.; Ramesh, A.; Kumar, S.; Nandi, D.; Brouillard, A.; Wells, A.; Pobezensky, L.; Osborne, B.; Kulkarni, A. A. Granzyme B nanoreporter for early monitoring of tumor response to immunotherapy. *Sci. Adv.* **2020**, *6* (40), No. eabc2777.
- (17) He, S. S.; Li, J. C.; Lyu, Y.; Huang, J. G.; Pu, K. Y. Near-infrared fluorescent macromolecular reporters for real-time imaging and urinalysis of cancer immunotherapy. *J. Am. Chem. Soc.* **2020**, *142* (15), 7075–7082.
- (18) Konishi, M.; Erdem, S. S.; Weissleder, R.; Lichtman, A. H.; McCarthy, J. R.; Libby, P. Imaging granzyme B activity assesses immune-mediated myocarditis. *Circ. Res.* **2015**, *117* (6), 502–512.
- (19) Larimer, B. M.; Wehrenberg-Klee, E.; Dubois, F.; Mehta, A.; Kalomeris, T.; Flaherty, K.; Boland, G.; Mahmood, U. Granzyme B PET imaging as a predictive biomarker of immunotherapy response. *Cancer Res.* **2017**, *77* (9), 2318–2327.
- (20) Scott, J. I.; Gutkin, S.; Green, O.; Thompson, E. J.; Kitamura, T.; Shabat, D.; Vendrell, M. A functional chemiluminescent probe for in vivo imaging of natural killer cell activity against tumours. *Angew. Chem., Int. Ed.* **2021**, *60* (11), 5699–5703.

- (21) Zhang, Y.; He, S. S.; Chen, W.; Liu, Y. H.; Zhang, X. F.; Miao, Q. Q.; Pu, K. Y. Activatable polymeric nanoprobe for near-infrared fluorescence and photoacoustic imaging of T lymphocytes. *Angew. Chem., Int. Ed.* **2021**, *60* (11), 5921–5927.
- (22) Wang, X. Q.; Danenberg, E.; Huang, C. S.; Egle, D.; Callari, M.; Bermejo, B.; Dugo, M.; Zamagni, C.; Thill, M.; Anton, A.; et al. Spatial predictors of immunotherapy response in triple-negative breast cancer. *Nature* **2023**, *621* (7980), 868–876.
- (23) Shi, Z. Y.; Du, Q.; Wang, X. F.; Wang, J. C.; Chen, H. X.; Lang, Y. L.; Kong, L. Y.; Luo, W. Q.; Yang, M.; Zhou, H. Y. Granzyme B in circulating CD8⁺ T cells as a biomarker of immunotherapy effectiveness and disability in neuromyelitis optica spectrum disorders. *Front. Immunol.* **2022**, *13*, 1027158.
- (24) Bhagchandani, S.; Johnson, J. A.; Irvine, D. J. Evolution of Toll-like receptor 7/8 agonist therapeutics and their delivery approaches: From antiviral formulations to vaccine adjuvants. *Adv. Drug Delivery Rev.* **2021**, *175*, 113803.
- (25) Frega, G.; Wu, Q.; Le Naour, J.; Vacchelli, E.; Galluzzi, L.; Kroemer, G.; Kepp, O. Trial Watch: Experimental TLR7/TLR8 agonists for oncological indications. *Oncoimmunology* **2020**, *9* (1), 1796002.
- (26) Stickdorn, J.; Stein, L.; Arnold-Schild, D.; Hahlbrock, J.; Medina-Montano, C.; Bartneck, J.; Ziss, T.; Montermann, E.; Kappel, C.; Hobernik, D.; et al. Systemically Administered TLR7/8 Agonist and Antigen-Conjugated Nanogels Govern Immune Responses against Tumors. *ACS Nano* **2022**, *16* (3), 4426–4443.
- (27) Aichhorn, S.; Linhardt, A.; Halfmann, A.; Nadlinger, M.; Kirchberger, S.; Stadler, M.; Dillinger, B.; Distel, M.; Dohnal, A.; Teasdale, I.; et al. A pH-sensitive macromolecular prodrug as TLR7/8 targeting immune response modifier. *Chem. - Eur. J.* **2017**, *23* (70), 17721–17726.
- (28) Wang, B.; Van Herck, S.; Chen, Y.; Bai, X. Y.; Zhong, Z. F.; Deswarte, K.; Lambrecht, B. N.; Sanders, N. N.; Lienenklaus, S.; Scheeren, H. W.; et al. Potent and prolonged innate immune activation by Enzyme-responsive imidazoquinoline TLR7/8 agonist prodrug vesicles. *J. Am. Chem. Soc.* **2020**, *142* (28), 12133–12139.
- (29) Lynn, G. M.; Laga, R.; Darrach, P. A.; Ishizuka, A. S.; Balaci, A. J.; Dulcey, A. E.; Pechar, M.; Pola, R.; Gerner, M. Y.; Yamamoto, A.; et al. In vivo characterization of the physicochemical properties of polymer-linked TLR agonists that enhance vaccine immunogenicity. *Nat. Biotechnol.* **2015**, *33* (11), 1201–1210.
- (30) Lynn, G. M.; Sedlik, C.; Baharom, F.; Zhu, Y. L.; Ramirez-Valdez, R. A.; Coble, V. L.; Tobin, K.; Nichols, S. R.; Itzkowitz, Y.; Zaidi, N.; et al. Peptide-TLR7/8a conjugate vaccines chemically programmed for nanoparticle self-assembly enhance CD8 T-cell immunity to tumor antigens. *Nat. Biotechnol.* **2020**, *38* (3), 320–332.
- (31) Wilson, D. S.; Hirosue, S.; Raczky, M. M.; Bonilla-Ramirez, L.; Jeanbart, L.; Wang, R. Y.; Kwissa, M.; Franetich, J. F.; Broggi, M. A. S.; Diaceri, G.; et al. Antigens reversibly conjugated to a polymeric glyco-adjuvant induce protective humoral and cellular immunity. *Nat. Mater.* **2019**, *18* (2), 175–178.
- (32) Yin, Q.; Luo, W.; Mallajosyula, V.; Bo, Y.; Guo, J.; Xie, J. H.; Sun, M.; Verma, R.; Li, C. F.; Constantz, C. M.; et al. A TLR7-nanoparticle adjuvant promotes a broad immune response against heterologous strains of influenza and SARS-CoV-2. *Nat. Mater.* **2023**, *22* (3), 380–390.
- (33) Hao, Y.; Li, H.; Ge, X.; Liu, Y.; Li, X.; Liu, Y.; Chen, H.; Zhang, S.; Zou, J.; Huang, L.; et al. Tumor-selective activation of Toll-like receptor 7/8 agonist nano-immunomodulator generates safe anti-tumor immune responses upon systemic administration. *Angew. Chem., Int. Ed.* **2022**, *61* (52), No. e202214992.
- (34) Casciola-Rosen, L.; Garcia-Calvo, M.; Bull, H. G.; Becker, J. W.; Hines, T.; Thornberry, N. A.; Rosen, A. Mouse and human granzyme B have distinct tetrapeptide specificities and abilities to recruit the bid pathway. *J. Biol. Chem.* **2007**, *282* (7), 4545–4552.
- (35) Tena-Solsona, M.; Alonso-de Castro, S.; Miravet, J. F.; Escuder, B. Co-assembly of tetrapeptides into complex pH-responsive molecular hydrogel networks. *J. Mater. Chem. B* **2014**, *2* (37), 6192–6197.
- (36) Panja, S.; Dietrich, B.; Shebanova, O.; Smith, A. J.; Adams, D. J. Programming Gels Over a Wide pH Range Using Multicomponent Systems. *Angew. Chem., Int. Ed.* **2021**, *60* (18), 9973–9977.
- (37) Yang, Z.; Liang, G.; Wang, L.; Xu, B. Using a kinase/phosphatase switch to regulate a supramolecular hydrogel and forming the supramolecular hydrogel in vivo. *J. Am. Chem. Soc.* **2006**, *128* (9), 3038–3043.
- (38) Yang, Z.; Liang, G.; Xu, B. Enzymatic hydrogelation of small molecules. *Acc. Chem. Res.* **2008**, *41* (2), 315–326.
- (39) Yu, Z. L.; Tantakitti, F.; Yu, T.; Palmer, L. C.; Schatz, G. C.; Stupp, S. I. Simultaneous covalent and noncovalent hybrid polymerizations. *Science* **2016**, *351* (6272), 497–502.
- (40) Li, I. C.; Hartgerink, J. D. Covalent capture of aligned self-assembling nanofibers. *J. Am. Chem. Soc.* **2017**, *139* (23), 8044–8050.
- (41) Zhang, Q. L.; Zheng, D. W.; Dong, X.; Pan, P.; Zeng, S. M.; Gao, F.; Cheng, S. X.; Zhang, X. Z. A strategy based on the enzyme-catalyzed polymerization reaction of Asp-Phe-Tyr tripeptide for cancer immunotherapy. *J. Am. Chem. Soc.* **2021**, *143* (13), 5127–5140.
- (42) Seia, M.; Zisman, E. Different roles of D-amino acids in immune phenomena. *FASEB. J.* **1997**, *11* (6), 449–456.
- (43) Freedman, B. R.; Uzun, O.; Luna, N. M. M.; Rock, A.; Clifford, C.; Stoler, E.; Östlund-Sholars, G.; Johnson, C.; Mooney, D. J. Degradable and removable tough adhesive hydrogels. *Adv. Mater.* **2021**, *33* (17), 2008553.
- (44) Fairbanks, B. D.; Schwartz, M. P.; Bowman, C. N.; Anseth, K. S. Photoinitiated polymerization of PEG-diacrylate with lithium phenyl-2,4,6-trimethylbenzoylphosphinate: polymerization rate and cytocompatibility. *Biomaterials* **2009**, *30* (35), 6702–6707.
- (45) Orgill, M.; Baker, B. L.; Owen, N. L. FTIR studies of conformational isomerism in acrylates and acrylic acids. *Spectrochim. Acta, Part A* **1999**, *55* (5), 1021–1024.
- (46) Arunkumar, R.; Drummond, C. J.; Greaves, T. L. FTIR spectroscopic study of the secondary structure of globular proteins in aqueous protic ionic liquids. *Front. Chem.* **2019**, *7*, 74.
- (47) Yang, F.; Shi, K.; Jia, Y. P.; Hao, Y.; Peng, J. R.; Qian, Z. Y. Advanced biomaterials for cancer immunotherapy. *Acta Pharmacol. Sin.* **2020**, *41* (7), 911–927.
- (48) Yang, C.; Wang, M.; Chang, M.; Yuan, M.; Zhang, W.; Tan, J.; Ding, B.; Ma, P. A.; Lin, J. Heterostructural nanoadjuvant CuSe/CoSe₂ for potentiating ferroptosis and photoimmunotherapy through intratumoral blocked lactate efflux. *J. Am. Chem. Soc.* **2023**, *145* (13), 7205–7217.
- (49) Chen, Y.; He, P.; Jana, D.; Wang, D.; Wang, M.; Yu, P.; Zhu, W.; Zhao, Y. Glutathione-depleting organic metal adjuvants for effective NIR-II photothermal immunotherapy. *Adv. Mater.* **2022**, *34* (21), No. e2201706.
- (50) Tokunaga, R.; Zhang, W.; Naseem, M.; Puccini, A.; Berger, M. D.; Soni, S.; McSkane, M.; Baba, H.; Lenz, H. J. CXCL₉, CXCL₁₀, CXCL₁₁/CXCR₃ axis for immune activation - A target for novel cancer therapy. *Cancer Treat Rev.* **2018**, *63*, 40–47.
- (51) Colombo, M. P.; Trinchieri, G. Interleukin-12 in anti-tumor immunity and immunotherapy. *Cytokine Growth Factor Rev.* **2002**, *13* (2), 155–168.
- (52) Roche, P. A.; Furuta, K. The ins and outs of MHC class II-mediated antigen processing and presentation. *Nat. Rev. Immunol.* **2015**, *15* (4), 203–216.
- (53) Steimle, V.; Siegrist, C.-A.; Mottet, A.; Lisowska-Grospierre, B.; Mach, B. Regulation of MHC Class II expression by interferon- γ mediated by the transactivator gene CIITA. *Science* **1994**, *265* (5168), 106–109.
- (54) Ivashkiv, L. B. IFN γ : Signalling, epigenetics and roles in immunity, metabolism, disease and cancer immunotherapy. *Nat. Rev. Immunol.* **2018**, *18* (9), 545–558.
- (55) Wei, Z. H.; Zhang, X. Q.; Yong, T. Y.; Bie, N. N.; Zhan, G. T.; Li, X.; Liang, Q. L.; Li, J. Y.; Yu, J. J.; Huang, G.; et al. Boosting anti-PD-1 therapy with metformin-loaded macrophage-derived microparticles. *Nat. Commun.* **2021**, *12* (1), 440.

(56) Zhang, F.; Parayath, N. N.; Ene, C. I.; Stephan, S. B.; Koehne, A. L.; Coon, M. E.; Holland, E. C.; Stephan, M. T. Genetic programming of macrophages to perform anti-tumor functions using targeted mRNA nanocarriers. *Nat. Commun.* **2019**, *10* (1), 3974.

(57) Ying, W.; Cheruku, P. S.; Bazer, F. W.; Safe, S. H.; Zhou, B. Y. Investigation of macrophage polarization using bone marrow derived macrophages. *J. Visualized Exp.* **2013**, *76*, 50323.

(58) Chen, D. S.; Mellman, I. Oncology meets immunology: The cancer-immunity cycle. *Immunity* **2013**, *39* (1), 1–10.

(59) Wang, F.; Su, H.; Xu, D.; Dai, W.; Zhang, W.; Wang, Z.; Anderson, C. F.; Zheng, M.; Oh, R.; Wan, F.; et al. Tumour sensitization via the extended intratumoural release of a STING agonist and camptothecin from a self-assembled hydrogel. *Nat. Biomed. Eng.* **2020**, *4* (11), 1090–1101.

(60) Korbecki, J.; Grochans, S.; Gutowska, I.; Barczak, K.; Baranowska-Bosiacka, I. CC chemokines in a tumor: A review of pro-cancer and anti-cancer properties of receptors CCR₅, CCR₆, CCR₇, CCR₈, CCR₉, and CCR₁₀ ligands. *Int. J. Mol. Sci.* **2020**, *21* (20), 7619.

(61) Fisher, D. T.; Appenheimer, M. M.; Evans, S. S. The two faces of IL-6 in the tumor microenvironment. *Semin. Immunol.* **2014**, *26* (1), 38–47.

(62) Castellino, F.; Huang, A. Y.; Altan-Bonnet, G.; Stoll, S.; Scheinecker, C.; Germain, R. N. Chemokines enhance immunity by guiding naive CD8⁺T cells to sites of CD4⁺T cell–dendritic cell interaction. *Nature* **2006**, *440* (7086), 890–895.